

## The Northwest Geysers EGS Demonstration Project, California: Pre-stimulation Modeling and Interpretation of the Stimulation

Jonny Rutqvist · Patrick F. Dobson · Julio Garcia · Craig Hartline · Pierre Jeanne · Curtis M. Oldenburg · Donald W. Vasco · Mark Walters

Received: 21 June 2013 / Accepted: 12 September 2013 / Published online: 17 October 2013  
© The Author(s) 2013. This article is published with open access at Springerlink.com

**Abstract** The Northwest Geysers Enhanced Geothermal System (EGS) demonstration project aims to create an EGS by directly and systematically injecting cool water at relatively low pressure into a known High Temperature (280–400 °C) Zone (HTZ) located under the conventional (240 °C) geothermal steam reservoir at The Geysers geothermal field in California. In this paper, the results of coupled thermal, hydraulic, and mechanical (THM) analyses made using a model developed as part of the pre-stimulation phase of the EGS demonstration project is presented. The model simulations were conducted in order to investigate injection strategies and the resulting effects of cold-water injection upon the EGS system; in particular to predict the extent of the stimulation zone for a given injection schedule. The actual injection began on October 6, 2011, and in this paper a comparison of pre-stimulation model predictions with micro-earthquake (MEQ) monitoring data over the first few months of a one-year injection program is presented. The results show that, by using a calibrated THM model based on historic injection and MEQ data at a nearby well, the predicted extent of the stimulation zone (defined as a zone of high MEQ density around the injection well) compares well with observed seismicity. The modeling indicates that the MEQ events are related to shear reactivation of preexisting fractures, which is triggered by the combined effects of injection-induced cooling around the injection well and small changes in steam pressure as far as half a kilometer away from the injection well. Pressure-monitoring data at adjacent wells and satellite-based ground-surface deformation data were also used to validate and further calibrate reservoir-scale hydraulic and mechanical model properties. The pressure signature monitored from the start of the injection was particularly useful for a precise back-calculation of

---

J. Rutqvist (✉) · P.F. Dobson · P. Jeanne · C.M. Oldenburg · D.W. Vasco  
Lawrence Berkeley National Laboratory (LBNL), Berkeley, CA 94720, USA  
e-mail: [Jrutqvist@lbl.gov](mailto:Jrutqvist@lbl.gov)

J. Garcia · C. Hartline · M. Walters  
Calpine Corporation, Middletown, CA 95461, USA

reservoir porosity. The first few months of reservoir pressure and surface deformation data were useful for estimating the reservoir-rock permeability and elastic modulus. Finally, although the extent of the calculated stimulation zone matches the field observations over the first few months of injection, the observed surface deformations and MEQ evolution showed more heterogeneous behavior as a result of more complex geology, including minor faults and fracture zones that are important for consideration in the analysis of energy production and the long-term evolution of the EGS system.

**Keywords** EGS · Modeling · Coupled processes · Geomechanics · Induced seismicity · Fluid injection

## 1 Introduction

The Geysers geothermal field in California (Fig. 1(a)) is the largest geothermal-electricity-generating operation in the world and has been in commercial production since 1960. It is a vapor-dominated geothermal reservoir system hydraulically confined by low-permeability rock units. As a result of high steam-withdrawal rates, the reservoir pressure declined from 1960 to the mid-1990s, when increasing water-injection rates resulted in a stabilization of the steam-reservoir pressure (Khan and Truschel 2010). In a portion of the northwestern part of The Geysers, exploratory drilling in the early 1980s discovered a relatively shallow high temperature zone (HTZ) with a conductive thermal gradient having temperatures ranging from 280 to 400 °C in low-permeability rock below the normal temperature (240 °C) steam reservoir (NTR). Note that the HTZ was originally called the high temperature reservoir (HTR) when it was first described by Walters et al. (1991). A number of steam production wells were drilled, but later abandoned because of economic problems caused by high concentrations of non-condensable gases (NCG) and highly corrosive hydrogen chloride gas in the steam. As result, the Northwest Geysers area, which contains a significant portion of the recoverable geothermal energy in the Geysers system is currently underutilized. In the ongoing Northwest Geysers EGS Demonstration Project (funded by the US Department of Energy's Geothermal Technologies Program and Calpine Corporation), the objective is to develop and demonstrate the technology required to extract energy from this type of low-permeability HTZ that typically underlies any high-temperature geothermal system.

One of the motivations for the project is the ample evidence that a large EGS was inadvertently created in the late 1970s below the oldest production area in the north-west part of The Geysers, when injected water reached the HTZ several kilometers below the deepest wells (Fig. 1(b)) (Stark 2003). Micro-earthquake (MEQ) and geochemical monitoring of this area indicates ongoing reactivation of fractures in the HTZ, and a temporal correlation of sustained steam production and lower NCG concentrations, especially since injection volumes increased when wastewater from the Santa Rosa Geysers Recharge Project began in 2003 (Stark et al. 2005). If a similar type of EGS could be created and successfully managed at the northwest Geysers, then large untapped resources could be utilized, with the potential to increase geothermal energy production at The Geysers. Thus, this type of EGS aims at enhancing

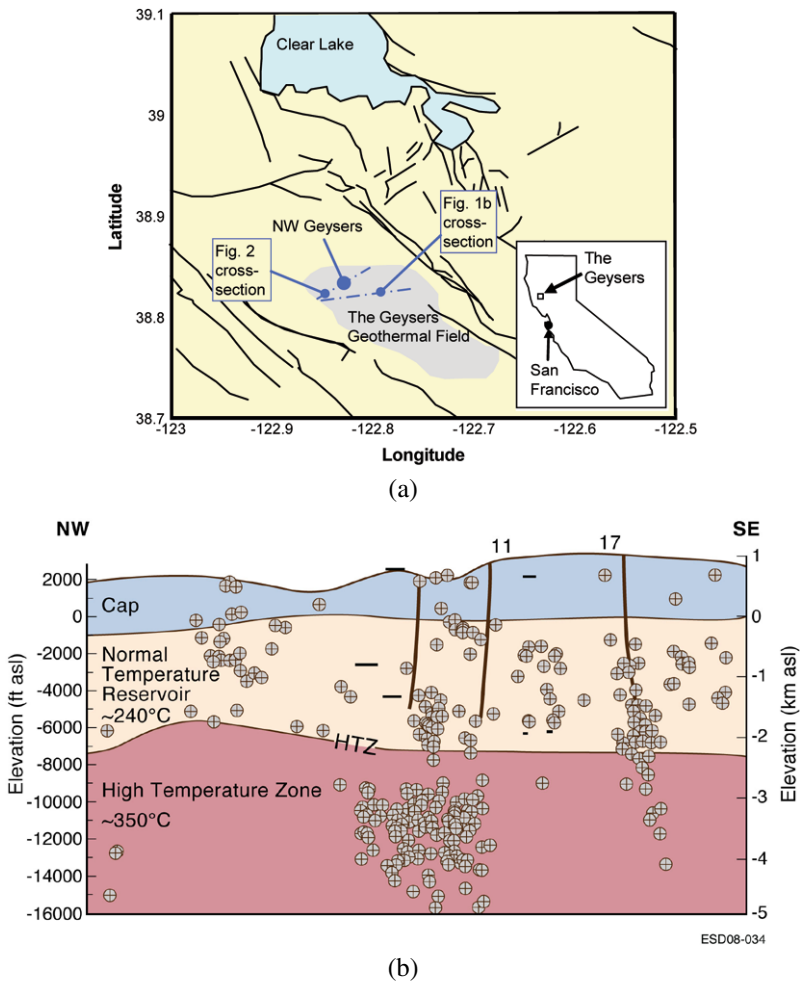


**Fig. 1** (a) Location of The Geysers Geothermal Field in California, and (b) NE-SW cross-section through the geothermal field showing 2002 MEQ hypocenters and injection wells (modified from Stark 2003)

the production beneath an existing conventional high-temperature geothermal steam field. The plan put forward for the Northwest Geysers EGS Demonstration Project was to reopen and recomplete two of the abandoned exploratory wells and deepen them for injection and stimulation in the HTZ, using injection water provided by the existing Santa Rosa Geysers Recharge pipeline. Using injection, the intention is to lower the NCG concentrations, stimulate existing fractures in the HTZ, and provide a sustainable amount of usable quality steam for production in line with a concept proposed by Nielson and Moore (2000).

The Northwest Geysers EGS Demonstration Project, launched in 2009, is organized into three phases: Phase I (Pre-Stimulation), Phase II (Stimulation), and Phase III (Monitoring). As a part of the prestimulation phase (Phase I) two of the abandoned exploration wells, Prati 32 (P-32) and Prati State 31 (PS-31) were success-

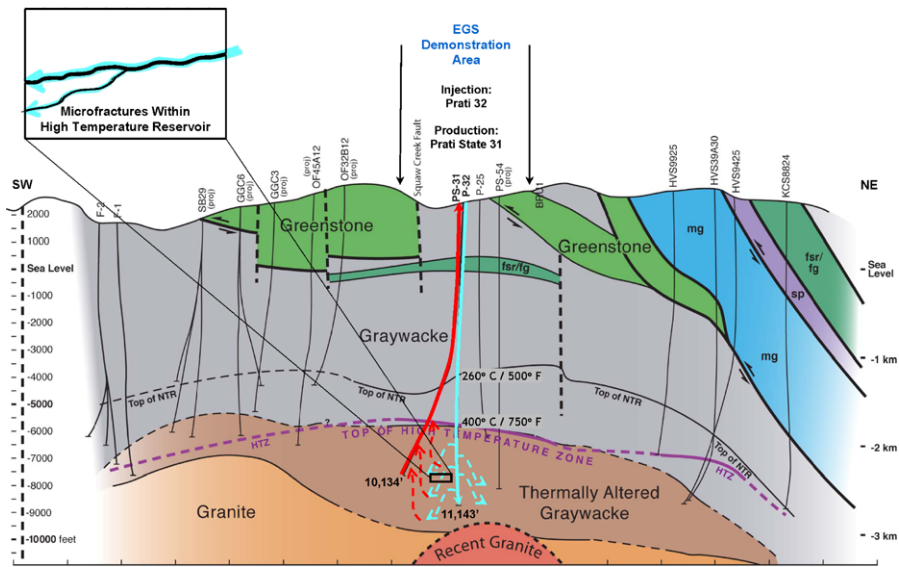
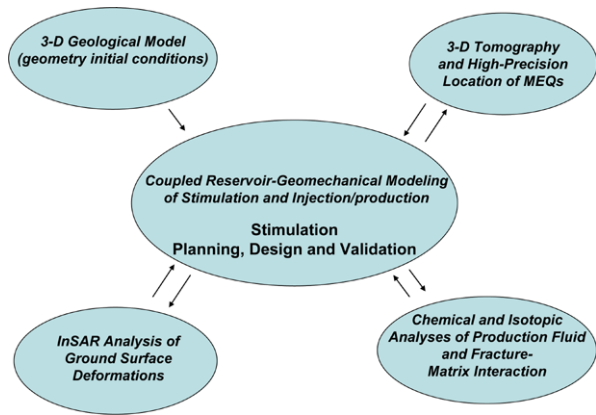


**Fig. 2** NE-SW geologic cross-section through the Northwest Geysers (see location in Fig. 1(a)) including the two wells P-32 and PS-31 that were reopened and recompleted as an injection/production pair within the HTZ (Garcia et al. 2012)

fully reopened, deepened, and recompleted as an injection-production pair (Fig. 2). With this deepening, the wells partially penetrate the HTZ over a depth ranging from about 3 to 3.5 km at a lateral distance of about 0.5 km from each other. More precisely, PS-31 was deepened to a measured depth of 3,058 m (10,034 ft), corresponding to a vertical depth of 2,929 m (9611 ft) below the ground surface. P-32 was deepened to a measured depth of 3,396 m (11,143 ft), corresponding to a vertical depth of 3,326 m (10,912 ft), with the temperature reaching an astonishing 400 °C at the base of the well. The P-32 injection well is cased to a vertical depth of 1,865 m (6,117 ft) and a blank (unperforated) liner is hung in the open hole below the casing down to a vertical depth of 2,564 m (8,411 ft). The blank liner is designed to prevent injection water from entering the NTR and aid injection directly into the HTZ below 2,564 m vertical depth. PS-31 is cased to 1,773 m (5,815 ft), and was completed as a production well with a slotted liner from a vertical depth of 2,066 m (6,776 ft) through the NTR and into the HTZ. In addition to the field work associated with the deepening and recompletion of the wells, the prestimulation project phase also involved site characterization and development of a stimulation plan. The stimulation phase (Phase II) of the project formally began on October 6, 2011, with the start of stimulation (i.e., the injection into P-32) using highly treated wastewater delivered by the Santa Rosa Geysers Recharge pipeline (Garcia et al. 2012). A one-year stimulation injection was conducted, systematically injecting cool water at carefully designed injection rates, keeping the bottom-hole pressure much below fracturing pressure, aiming at a gentle but pervasive stimulation of an existing fracture network. The final monitoring phase (Phase III), involves monitoring and analysis of the long-term sustainability of the system during continuous injection and production from the EGS.

**Fig. 3** Coupled THM modeling integrated with field monitoring associated with the Northwest Geysers EGS demonstration project



In the EGS demonstration project, coupled thermal, hydraulic, and mechanical (THM) modeling is integrated with field monitoring for planning, design, and validation of the EGS (Fig. 3). As part of this work, the coupled THM modeling is used to (1) gain insight into the underlying mechanisms of MEQ events and their potential role in enhancing permeability of the proposed EGS reservoir, and (2) to investigate injection strategies and their effects upon the EGS system. The MEQ activity is monitored by an existing seismic array which was also used to collect background data prior to the injection. Closely monitoring the spatial and temporal evolution of the MEQ activity could serve as an effective method of remotely sensing the development of the enhanced fracture volume, and may provide constraints on the conceptual model. In addition to real-time MEQ monitoring and analysis, the field monitoring and data analyses also include (1) three-dimensional tomography and high-precision location source studies of MEQ events, (2) satellite-based monitoring of ground-surface deformation, and (3) geochemical monitoring analysis of injection and production fluids (Fig. 3). These technologies are promising for monitoring and validating the EGS, because they are expected to capture important changes in the geothermal reservoir at the kilometer scale, including changes in rock-mass mechanical properties (as reflected by changes in sonic velocities) and exposure of new fracture surfaces (as reflected by changes in the chemical signature of the produced steam). In addition to these tools, the demonstration wells are repeatedly logged with a pressure-temperature-spinner (PTS) tool to evaluate changes in reservoir properties near the wellbores (Garcia et al. 2012).

This paper presents coupled THM numerical modeling conducted as part of the prestimulation phase (Phase I) for guiding the stimulation plan. In particular, the prestimulation modeling aimed at predicting the injection-induced spatial extent, or volume, of the stimulation zone and the associated zone of MEQ activity around the wells. Model results are compared with the first few months of Phase II field monitoring data, including MEQ spatial evolution, reservoir pressure (from monitoring in the PS-31 well), and ground-surface deformations (from satellites). It is shown that the prestimulation modeling using a simplified representation of geology could predict the lateral extent of the stimulation zone encompassing the injection/production well

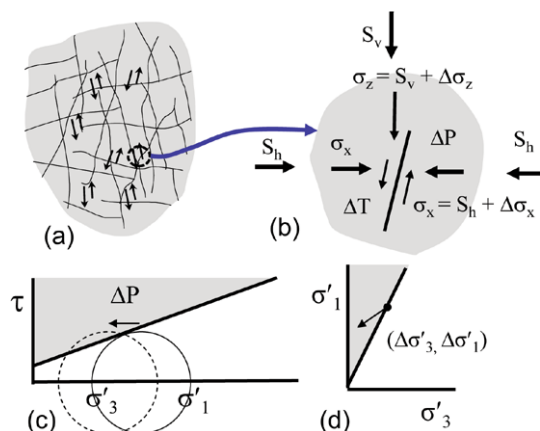
pair, although field data indicate the influence of more complex geological structures that will be included in future models of the field.

## 2 Modeling Approach

The coupled THM analysis was conducted with TOUGH-FLAC (Rutqvist et al. 2002; Rutqvist 2011), a simulator based on linking the geothermal reservoir simulator TOUGH2 (Pruess et al. 2011) with the geomechanical code FLAC3D (Itasca 2009). The simulator has the required capabilities for modeling of coupled THM responses caused by injection and production under complex multiphase flow and thermal processes within the steam-dominated geothermal system at The Geysers. The application of this simulator to the Northwest Geysers EGS Demonstration Project follows for the approach first used in previous Geysers studies by Rutqvist and Oldenburg (2007, 2008). The simulation involves modeling the fractured rock mass using a continuum approach, in which fractures are represented implicitly using equivalent hydraulic and mechanical properties.

One of the main features of the geomechanical modeling approach applied in this study is the analysis of injection-induced stress changes and the potential for shear reactivation of fractures in a rock mass which is near critical stress for shear failure (Fig. 4). The concept of a critically stressed rock mass at The Geysers dates back to rock-mechanical studies conducted in the early 1980s indicating that the reservoir rock has undergone extensive hydrothermal alteration and recrystallization, and that it is highly fractured (Lockner et al. 1982). Based on laboratory studies, Lockner et al. (1982) suggested that hydrothermal alteration and fracturing has weakened the reservoir rock at The Geysers to such an extent that models of the geothermal field should assume that only a frictional sliding load can be supported by the rock, and that shear stress in the region is probably near the rock-mass frictional strength. Therefore, small perturbations of the stress field by fluid injection (for example) could trigger seismicity. The potential for shear slip is evaluated using a Mohr–Coulomb failure criterion under the conservative assumption that fractures of any orientation could

**Fig. 4** Illustration of the approach for failure analysis to evaluate the potential for induced seismicity at The Geysers, including (a) highly fractured rock with randomly oriented fractures, (b) changes in stress on one fracture plane, (c) movements of Mohr's circle as a result of increased fluid pressure within a fracture plane for a critically stressed fracture, and (d) corresponding stress path in the  $(\sigma'_1, \sigma'_3)$  plane



exist anywhere (Fig. 4(a)). Such an assumption is supported by studies of fault-plane analysis of seismicity at The Geysers by Oppenheimer (1986), which indicated that seismic sources occur from almost randomly oriented fracture planes. Under this assumption, the isotropic Mohr–Coulomb criterion can be used and can be stated in terms of maximum and minimum compressive effective stresses, such as Jaeger and Cook (1979)

$$\sigma'_1 = C_0 + q\sigma'_3, \quad (1)$$

where  $C_0$  is the uniaxial compressive strength and  $q$  is the slope of the  $\sigma'_1$  versus  $\sigma'_3$  line, which is related to the coefficient of friction,  $\mu$  according to

$$q = [(\mu^2 + 1)^{\frac{1}{2}} + \mu]^2. \quad (2)$$

The criterion in Eq. (1) is used in this paper, to follow the simulated time-evolution of the principal ( $\sigma'_1, \sigma'_3$ ) stress path in relation to the principal stresses required for failure.

One key parameter in estimating the likelihood of shear reactivation along a fracture is the coefficient of static friction,  $\mu$ , entering the Coulomb shear failure criterion through Eq. (2). Cohesionless faults are usually assumed to have a friction coefficient of 0.6 to 0.85; and a frictional coefficient of  $\mu = 0.6$  is a lower-limit value observed in fractured rock masses associated with shear-enhanced permeability (Barton et al. 1995). For  $\mu = 0.6$  and zero cohesion, the rock-mass uniaxial compressive stress term,  $C_0$  in Eq. (1) vanishes and the Coulomb criterion for the onset of shear failure can be written as

$$\sigma'_{1c} = 3\sigma'_3, \quad (3)$$

where  $\sigma'_{1c}$  is the critical maximum principal compressive stress for the onset of shear failure, and the factor 3 is a result of the frictional coefficient of  $\mu = 0.6$  in Eq. (2). Thus, according to Eq. (3), shear reactivation would be induced at a point in the rock mass whenever the maximum principal effective compressive stress is three times higher than the minimum principal compressive stress.

Based on the concept of a critically stressed rock mass, the initial stress will be in a state of incipient failure (Figs. 4(b), (c), and (d)). By studying how the stress state deviates from this near-critical stress state, the intent is to investigate whether the changes in the local stress state tend to move the system toward a state of failure or away from failure. The likelihood of shear reactivation would increase if the change in maximum principal compressive effective stress is more than three times the change in minimum principal compressive effective stress (i.e.,  $\Delta\sigma'_1 \geq 3 \times \Delta\sigma'_3$ ). Conversely, the likelihood of shear reactivation would decrease if the change in maximum principal compressive effective stress were less than three times the change in minimum principal compressive effective stress (i.e., if  $\Delta\sigma'_1 < 3 \times \Delta\sigma'_3$ ).

Considering that the initial stress might not be exactly at the state of critical stress, one may quantify how much the  $\Delta\sigma'_1$  has to exceed  $3 \times \Delta\sigma'_3$  in order to trigger shear reactivation. Therefore, a stress-to-strength change is defined as  $\Delta\sigma'_{1m} = \Delta\sigma'_1 - 3 \times \Delta\sigma'_3$ , and a critical stress-to-strength change  $\Delta\sigma'_{1mc}$  when shear reactivation would be induced. Thus, the criterion for inducing shear reactivation would be  $\Delta\sigma'_{1m} \geq \Delta\sigma'_{1mc}$ . In this study,  $\Delta\sigma'_{1mc}$  was quantified by model calibration against historic injection

and MEQ data from the Aidlin 11 well, located in the Northwest Geysers, a few kilometers west of the EGS demonstration area (Majer and Peterson 2007). Moreover, the parameter  $\Delta\sigma'_{1m}$  is defined as the MEQ potential, indicating that a higher  $\Delta\sigma'_{1m}$  is equivalent to a higher MEQ potential. That is, the higher the  $\Delta\sigma'_{1m}$ , the higher the likelihood of triggering a seismic event. One advantage of this approach is that it is not a requirement to know the exact absolute magnitude and direction of the in situ stress field, which are parameters notoriously difficult to measure, especially in hot geothermal environments. Instead, one may assume that the stress field is near critically stressed, look at injection-induced changes in stress, and calibrate the model at the nearby well in a similar environment with a similar in situ stress field. It is expected that similar stress changes will be required to induce MEQ events at the nearby wells. However, the exact extent of the stimulation zone will depend on the injection schedule, which can be simulated using the coupled THM model.

The adopted approach should be viewed as a pragmatic method for estimating the extent to the stimulation zone based on the calculated injection-induced stress perturbations, recognizing that the underlying complex three-dimensional stress and fracture interactions are not considered in detail. For example, a local shear stress drop associated with the reactivation of a fracture might trigger shear in nearby fractures or fracture surface areas as well as relieve stresses to prevent further reactivation at the same locations (Catalli et al. 2013; McClure and Horne 2012). Detailed analysis of such processes would require explicit representation of individual fractures in the model (McClure and Horne 2012). Nevertheless, the approach adopted in this study is considered sufficient for estimating the extent of the stimulation zone using model calibration against historic injection and MEQ data at a nearby well.

### 3 THM Input Parameters

The various coupled THM models of The Geysers used in this study consist of the relatively permeable NTR sandwiched between an impermeable cap on top and a relatively low-permeability HTZ at depth, as outlined in Fig. 1(b) and shown in more detail for the Northwest Geysers in Fig. 2. The main geologic units of the models include (1) unfractured graywacke that serves as a caprock, (2) metagraywacke (host to the NTR), (3) hornfelsic graywacke (hornfels), and (4) young (<1 Ma) granitic intrusive rocks (felsite), which are thought to be as young as about 10,000 years before the present (Williams et al. 1993), and the heat source to the HTZ in the EGS demonstration area (Walters et al. 1988; Sternfeld 1989; Schmitt et al. 2003) (Fig. 2). The initial thermal and hydrological conditions (vertical distributions of temperature, pressure, and liquid saturation) for each model are typically established through steady-state, multiphase flow simulations. In the models used in this study, the initial reservoir temperature in the NTR is approximately 240 °C down to a depth of about 2.5 km, and then gradually increases up to 370 °C toward the bottom boundary at a depth of 6 km. Note that the temperatures at depth used in the prestimulation model of the EGS area are somewhat cooler than the very high temperature that was later encountered at the base of the P-32 well. A relatively low permeability of the HTZ below the NTR can be inferred from a steep thermal gradient across the HTZ, which indicates a



**Table 1** Rock properties for modeling of the initial injection at the Northwest Geysers EGS demonstration project

	Caprock	Graywacke (NTR)	Hornfels (HTZ)	Felsite (HTZ)
Permeability ( $\text{m}^2$ )	$1 \times 10^{-18}$	$5 \times 10^{-14}$	$2 \times 10^{-14}$	$1 \times 10^{-15}$
Porosity (–)	0.01	0.015	0.01	0.01
Thermal Cond. ( $\text{W}/(\text{m } ^\circ\text{C})$ )	3.2	3.2	3.2	3.2
Specific heat ( $\text{J}/(\text{kg } ^\circ\text{C})$ )	1000	1000	1000	1000
Bulk modulus (GPa)	3.3	3.3	3.3	3.3
Shear modulus (GPa)	2	2	2	2
Thermal expansion coefficient ( $^\circ\text{C}^{-1}$ )	$1 \times 10^{-5}$	$1 \times 10^{-5}$	$1 \times 10^{-5}$	$1 \times 10^{-5}$

lack of heat convection and heat transport only through conduction. At The Geysers, the steam pressure within the hydraulically confined NTR has gradually decreased with steam production since the 1960s, and is today a few megapascals; thus, the initial reservoir pressure in the model simulations related to the new EGS and injection is a few megapascals.

Table 1 presents the basic THM properties for the different model units. The permeability and porosity values of the NTR are taken from Calpine's reservoir model, whereas permeability and porosity are lower for the HTZ, extending from the hornfelsic graywacke down into the felsite. The geomechanical properties are equivalent to those developed and used by Rutqvist and Oldenburg (2007, 2008) in previous modeling of The Geysers field-wide coupled THM responses. This includes a rock-mass bulk modulus,  $K = 3.3$  GPa, which approximately corresponds to values back-calculated by Mossop and Segall (1997) based on reservoir-scale strain analyses of production-induced subsidence. The linear thermal expansion coefficient of the rock is set to  $1 \times 10^{-5} \text{ } ^\circ\text{C}^{-1}$ , corresponding to values determined from core samples of the reservoir rock at high ( $250 \text{ } ^\circ\text{C}$ ) temperature (Mossop and Segall 1997). Using these properties, Rutqvist and Oldenburg (2007, 2008) simulated, in a vertical section across the central part of The Geysers, the first 44 years of field-wide production and injection from the early 1960s. These coupled THM simulations resulted in reservoir-wide pressure and temperature declines of a few MPa and a few degrees, respectively, as well as subsidence of about 0.5 to 1 meter. These numbers are in general agreement with field observations at The Geysers (Williamson 1992; Mossop and Segall 1997). Moreover, in Rutqvist (2011), this model was further validated by comparing the calculated transient subsidence in the central part of The Geysers field with subsidence data obtained from satellite-based synthetic aperture radar (SAR) data over a seven-year period, from 1992 to 1999. Figure 5(a) shows the observed average yearly range change (changes in distance between the satellite and ground surface in the line-of-sight) derived using C-band data from the European Space Agency's (ESA) ERS-1 and ERS-2 SAR satellites. The data points shown in Fig. 5(a) were developed on behalf of LBNL by Tele-Rilevamento Europa (TRE) in Italy, using the permanent scatterer (PS) technique (Ferretti et al. 2001). The PS technique uses individual radar-bright and phase-stable objects on the Earth's surface (scatterers) to determine a time-series for the displacement of each scatterer projected

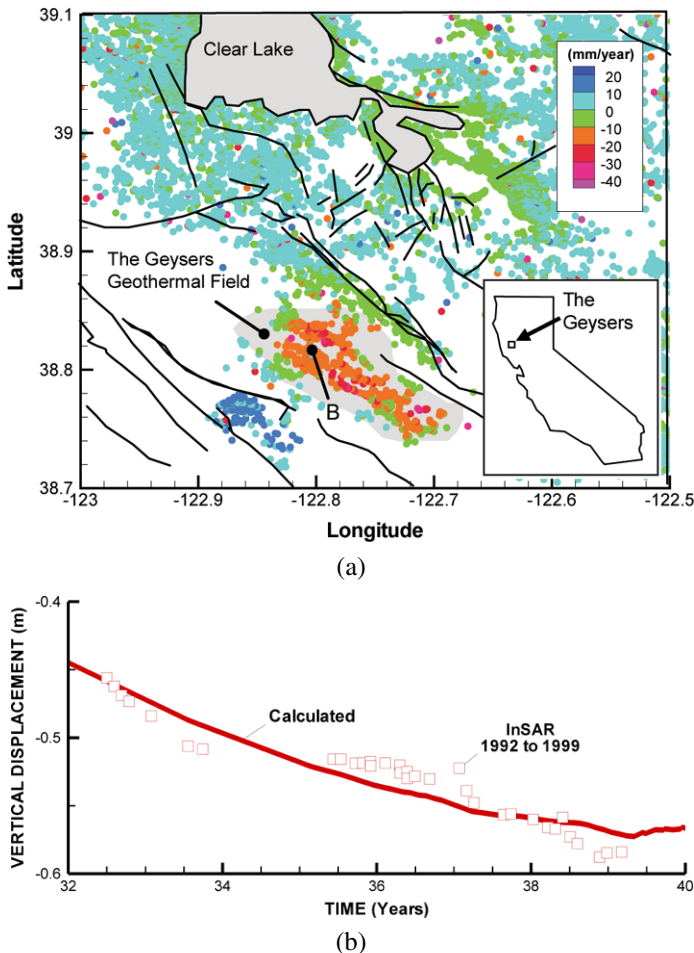


**Fig. 5** (a) InSAR data of rate of average yearly range change (changes in distance between the satellite and ground surface in the line-of sight), which are close to vertical displacement at The Geysers during 1992 to 1999, and (b) comparison of calculated vertical displacements with range change at the center of the subsidence bowl (Point B) from year 32 to 40 (1992 to 1999) since the start of the steam production in 1960 (Rutqvist 2011)

onto the satellite's line-of-sight. Because of a steep look angle ( $23^\circ$  relative to vertical), the range change estimates shown in Fig. 5(a) are sensitive primarily to vertical displacement.

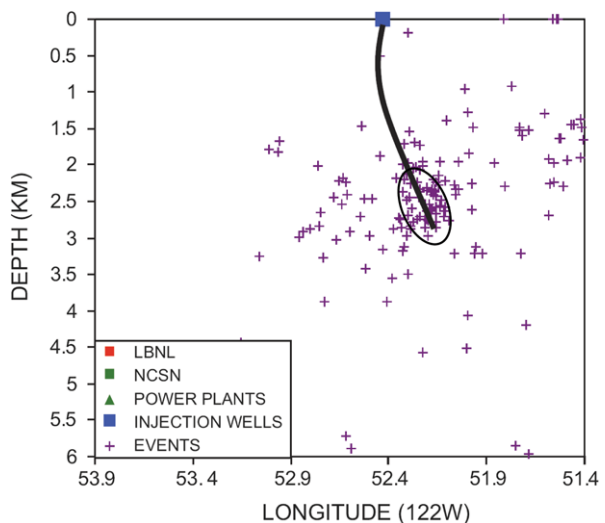
Figure 5(b) shows very good agreement between the calculated and observed time-evolution of subsidence at the center of the subsidence bowl. These TOUGH-FLAC model simulations, as well as the previous studies by Mossop and Segall (1997), indicated that the subsidence is caused by poroelastic compaction related to net mass extraction of fluid from the geothermal reservoir, and that the magnitude of subsidence can be matched using a rock-mass bulk modulus of 3.3 GPa. Note, however, that the rock mass bulk modulus of 3.3 GPa (which appears to be a low value for

this type of rock and at this depth) might in reality represent the tangent modulus of inelastic compaction of the reservoir rock. Moreover, subsidence can also occur as a result of reservoir cooling, a process that was considered in Rutqvist and Oldenburg (2007, 2008). However, if the field-wide cooling is only a few degrees, the subsidence caused by thermal contraction would be negligible. The notion that subsidence is driven by poroelastic compaction rather than cooling contraction is also supported by the fact that the largest magnitude of subsidence occurred in areas with the most substantial pressure depletions (Mossop and Segall 1997).

#### 4 Calibration of MEQ Criterion by Modeling Aidlin 11 Injection

Historic injection and the MEQ data at the Aidlin 11 injection well, located about 5 km to the west of the EGS demonstration area, was analyzed and modeled for calibration of the critical stress-to-strength change,  $\Delta\sigma'_{lmc}$ . At Aidlin 11, the injection takes place at a depth of 3.5 km near the NTR/HTZ interface. Injection began in late 2004 at a relatively low rate of 100 to 200 gpm. The injection rate was held relatively steady until September 2005, when it was sharply increased (Majer and Peterson 2007). The results of detailed MEQ monitoring within a 6 km cube containing the Aidlin 11 injection well was published by Majer and Peterson (2007). Figure 6 shows an east-west cross section through the center of the cluster, as well as the trace of the well. The seismicity during the first year of constant-rate injection was concentrated near the bottom the well. Some of the sparse seismicity away from the injection well may be associated with production wells in the area. The response to injection in Aidlin 11 was simulated using a three-dimensional model domain that is one-quarter of a 2 km × 2 km block in the horizontal plane and 5.5 km deep. For the model calibration, the injection and MEQ activities for the first year were considered when injection took place at a relatively constant rate. In the modeling, a constant

**Fig. 6** E-W projection through a 6 km cube containing MEQ hypocenters of magnitude 0.8 or larger during 1 year of injection at Aidlin 11 (from Majer and Peterson 2007)



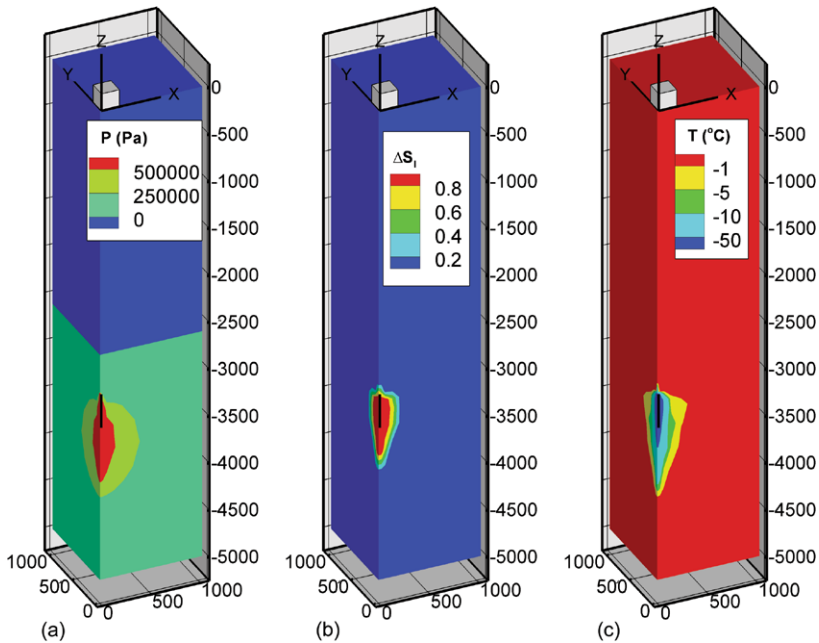
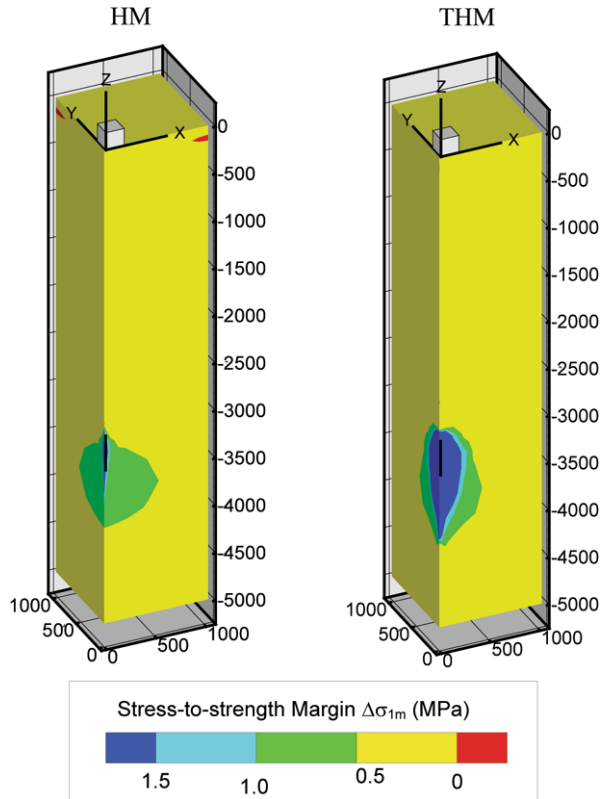


**Fig. 7** Simulation results of after 1 year of water injection at Aidlin 11: Changes in (a) fluid pressure, (b) liquid saturation, (c) temperature after 1 year of injection (with scales along  $x$ ,  $y$ ,  $z$ -axes in meters)

average injection rate of 7.7 kg/s (122 gpm) and a bottom-hole injection temperature of 90 °C were maintained for 1 year. In these model simulations, the initial reservoir temperature at the bottom of the Aidlin 11 was about 275 °C, and the steam pressure was 4 MPa.

Figure 7 shows the calculated changes in pressure, liquid saturation, and temperature after 1 year of injection in Aidlin 11, whereas Fig. 8 shows the resulting MEQ potential ( $\Delta\sigma'_{1m}$ ). In general, the temperature change is several tens of degrees, but is confined within the zone of liquid water migrating downward from the bottom of the injection well. The pressure change is only a few MPa, but takes place far beyond the extent of the liquid water zone. Figure 8 presents the resulting MEQ potential ( $\Delta\sigma'_{1m}$ ) for considering THM coupling and only HM coupling. One can observe that when considering full THM coupling,  $\Delta\sigma'_{1m}$  is higher and the zone of high  $\Delta\sigma'_{1m}$  tends to spread farther downward. The calculated results in Fig. 8 can be compared to the observed MEQ cloud (depicting events with  $M \geq 0.8$ ) around the Aidlin 11 (Fig. 6). The extent of the higher-density MEQ cloud around Aidlin 11 roughly corresponds to the extent of the blue contours (dark blue or light blue) for the THM model. The dark-blue contour corresponds to a zone with  $\Delta\sigma'_{1m} > 1.5$  MPa. This means that in the zone where maximum compressive effective stress has increased by 1.5 MPa or more relative to compressive strength, a relatively high density of MEQ events with  $M \geq 0.8$  was triggered by the injection. One may define this zone of high-density MEQ activity as the stimulation zone, with its extent corresponding to the critical stress-to-strength change,  $\Delta\sigma'_{1mc} = 1.5$  MPa.

**Fig. 8** Simulation results of MEQ potential for Aidlin 11 area estimated using the stress-to-strength margin,  $\Delta\sigma_{1m}$ , for HM and THM couplings considered (with scales along  $x, y, z$ -axes in meters)



**5 Model Predictions of the Stimulation Zone at Prati 32 (P-32)**

For modeling the P-32 injection, another simplified yet representative model of the geology in the field was developed, this time focusing on the geological units around the EGS area (Fig. 9). For example, all relevant geological units and the two wells were included, but the geometry was simplified by extending geological layers horizontally to model boundaries, and by assuming perfectly vertical wells. This simplified model is considered sufficient for making a first-order estimate of the temporal and spatial extent of the stimulation zone (corresponding to the extent of the high density MEQ zone). In this model prediction, the same THM model approach and material parameters that were back-calculated from the previous field-wide THM analysis at Aidlin 11 were used. Moreover, the critical stress-to-strength change ( $\Delta\sigma'_{1mc} = 1.5$  MPa) that was back-calculated from historic injection and MEQ data at Aidlin 11 was applied for predicting the extent of the stimulation zone. Using this model, the likely extent of the stimulation zone was evaluated for a number of injection scenarios, including injection consecutively in PS-31 and P-32 for 6 months each (see Rutqvist et al. 2010), or injection for 12 months in PS-31 only, or P-32 only. The final stimulation plan, which corresponds to the injection scenario analyzed and presented in this paper, involved injection into the deeper and hotter P-32 well, with step-wise increases and decreases of the injection rates over a 1-year injection period.

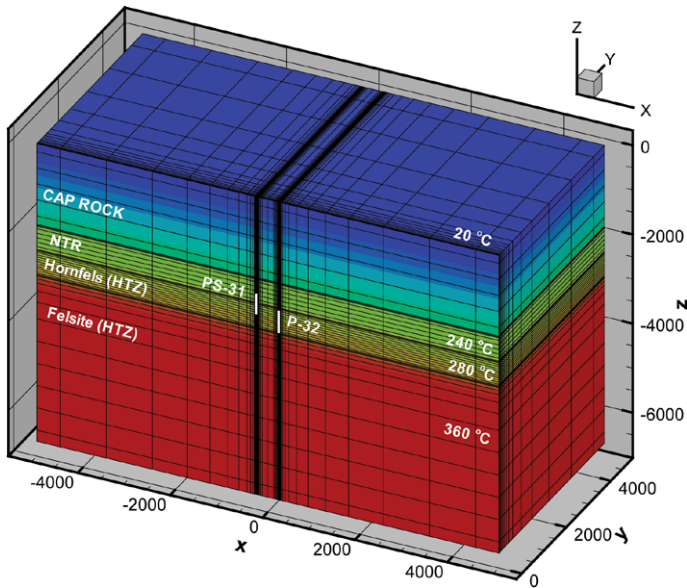
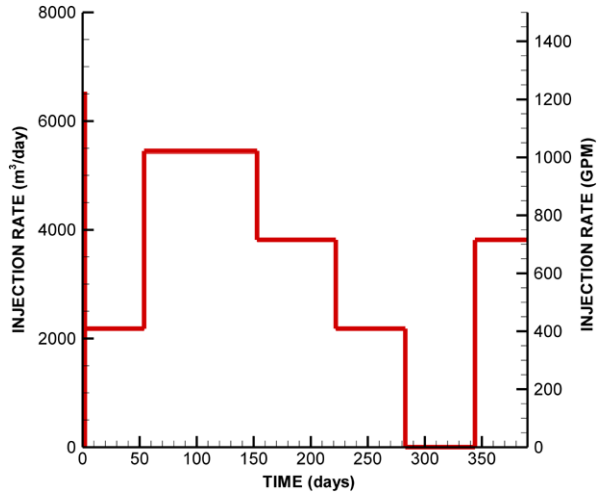


**Fig. 9** Three-dimensional numerical grid with material layers and contours of initial temperature.  $x$  = NS model dimensions and  $y$  = EW model dimension with origin located at  $x = 176087.581$  feet and  $y = 427583.966$  feet in California Lambert coordinates (scales along  $x$ ,  $y$ ,  $z$ -axes are model dimensions in meters)

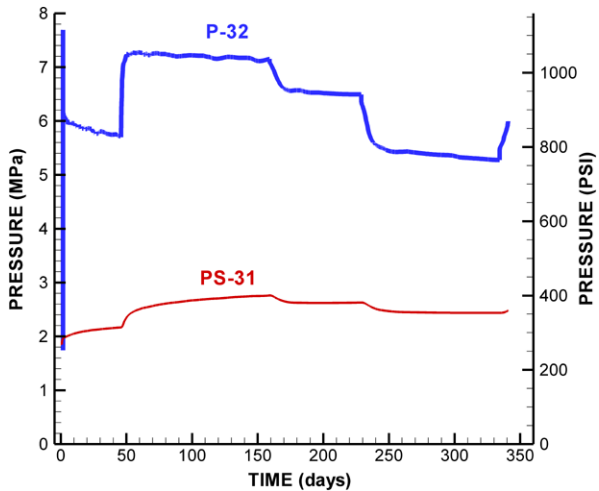
Figure 10 presents modeling results of well pressures in the two wells for the injection into P-32 following the injection scheme defined in the final stimulation plan. First, there is an initial 24-hour period of relatively high-rate injection of 1200 gpm (gallons per minute) that is necessary to collapse the steam bubble in the well bore and nearby formation, so that relatively lower sustained rates of liquid water injection are drawn into the fractured reservoir rock under vacuum. Thereafter, the injection scheme consists of steps over several months of increasing and decreasing rates. The simulated maximum bottom-hole pressure during these steps is less than 8 MPa at the base of P-32 (Fig. 10(b)). In the field, this corresponds to a water head of 800 m at 3326 m depth (base of the P-32 well), leading to a water column in P-32 with the free water surface at a depth of 2536 m or at an elevation of 1882 m bsl. This means, as can be noted from the geologic cross section in Fig. 2, that the injection (in theory) took place below the NTR, into the hornfelsic graywacke, which corresponds to the upper part of the HTZ. At the injection depth, the least compressive stress magnitude may be bounded to be at least 24 MPa, using a conservative frictional strength limit of the rock mass. Thus, the predicted maximum bottom-hole pressure of 8 MPa is much less than the least principal compressive stress, and therefore far below the fluid pressure that would be required for creating new hydraulic fractures through tensile failure. Thus, by injecting at a low pressure, single hydraulic fracture propagation is avoided, instead aiming at creating a more pervasive stimulation zone by dilating a network of preexisting fractures through shear reactivation.

Figure 11 shows predicted changes in pressure and temperature after 3 months (90 days) of injection, while Fig. 12 shows predicted changes in stress parameters

**Fig. 10** Injection rates (a) and calculated downhole pressure evolution (b) for the proposed injection schedule

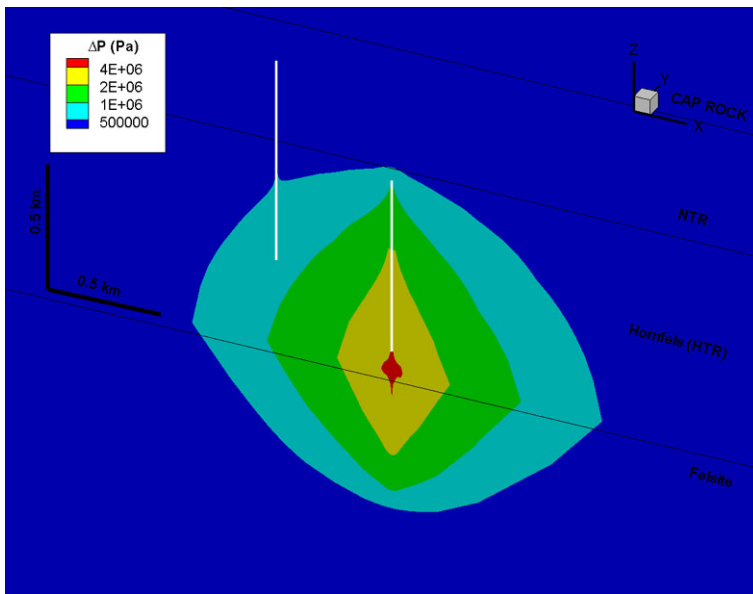


(a)

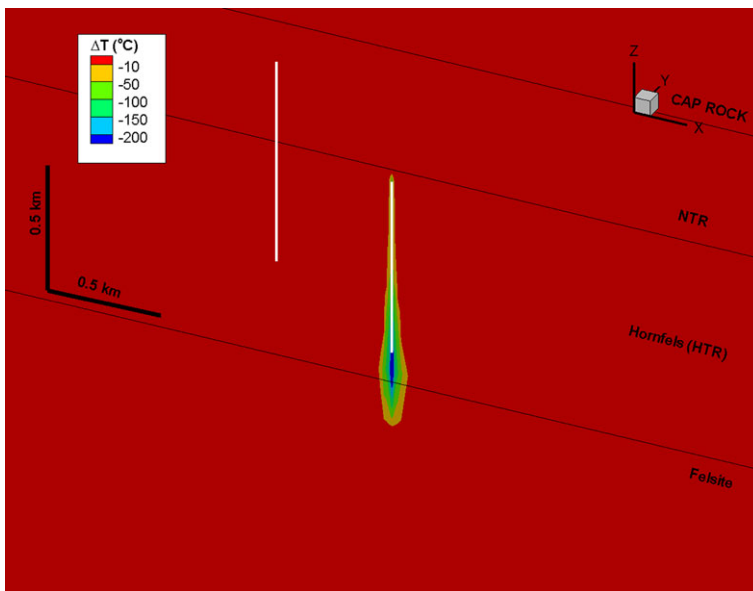


(b)

and MEQ potential. At 90 days, the injection rate has been sustained at the highest rate of 1,000 gpm for about 1 month. Despite the injection rate being the highest, the pressure increase around the injection well is only a few megapascals (Fig. 11(a)). At the same time, substantial cooling is observed below the injection well, which coincides with a zone of liquid water from the injection (Fig. 11(b)). Figure 12(c) shows the MEQ potential in terms of stress-to-strength change ( $\Delta\sigma'_{1m}$ ) after 90 days of injection. Recall that the critical stress-to-strength change was estimated to be  $\Delta\sigma'_{1mc} = 1.5$  MPa through back-analysis by modeling injection at the nearby Aidlin 11 well.  $\Delta\sigma'_{1m} = 1.5$  MPa or higher corresponds to the blue contour in Fig. 12(c), which is therefore the predicted extent of the stimulation zone. In Fig. 12(c), the blue contour extends about 0.5 km from the P-32 injection well, barely reaching the PS-



(a)

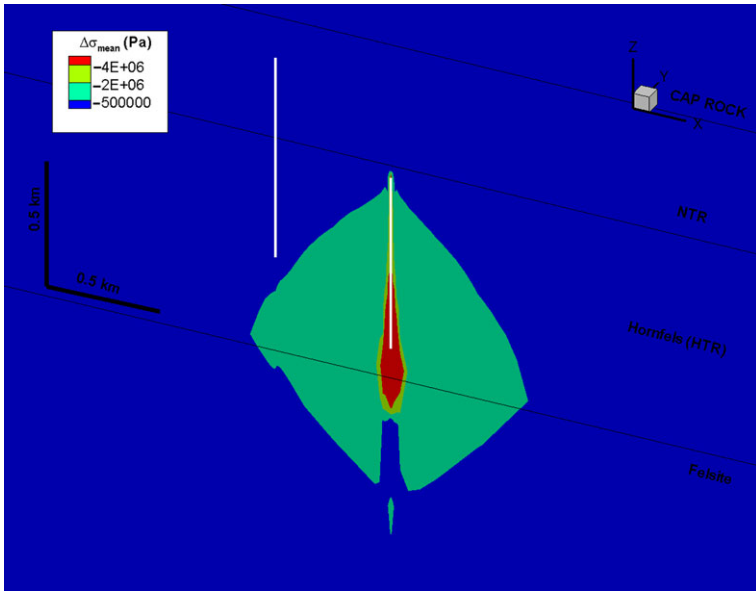


(b)

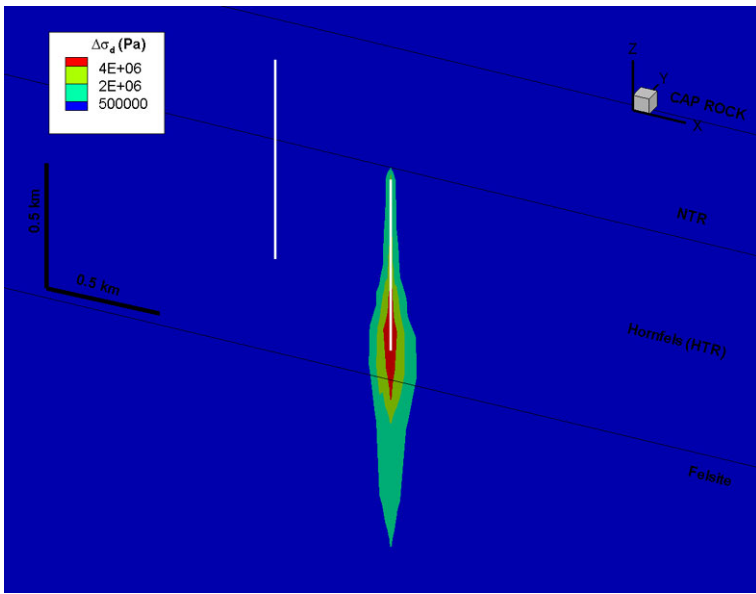
**Fig. 11** Predicted changes in (a) pressure, and (b) temperature after 3 months of injection

31 well. However, modeling of the continued injection beyond 90 days shows that the zone of high MEQ density would continue to grow to encompass the PS-31 well before the end of the 1-year injection campaign. A closer examination at the sim-





(a)



(b)

**Fig. 12** Predicted changes in (a) effective mean compressive stress, (b) shear stress, and (c) MEQ potential in terms of stress-to-strength margin after 3 months of injection

ulation results in Fig. 12 indicates that reduction in effective stress, with unloading of preexisting fractures and associated loss of shear resistance, would likely be the mechanism leading to shear reactivation and MEQ events around the injection well.

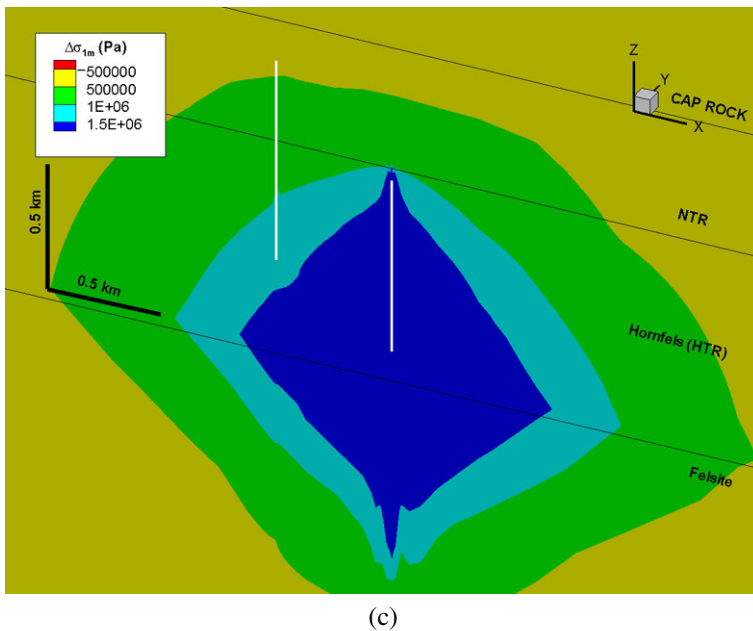
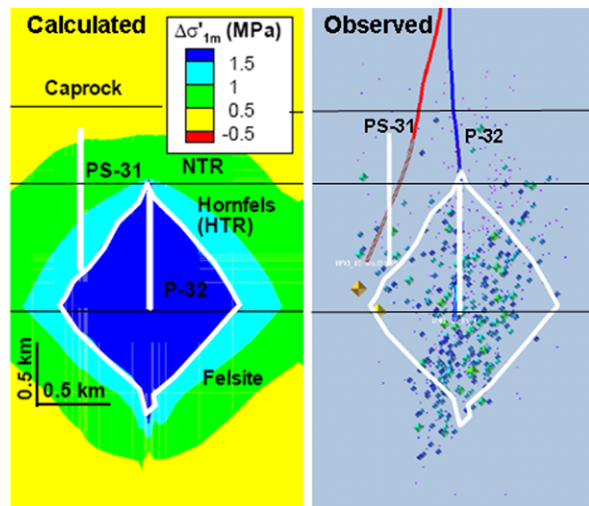


**Fig. 12** (Continued)

This is illustrated by the similarity in the shape of the high potential MEQ zone in Fig. 12(c) and the zone of reduced effective compressive stress in Fig. 12(a). One can also see that this reduction in effective compressive stress (a reduction of about 0.5 MPa or more) correlates with the zone of a pressure increase of more than 1 MPa in Fig. 11(a). Moreover, from comparison of Figs. 12(b) and 11(b), it is observed that high shear stress is developed close to the zone of cooling around and below the injection well. This indicates that the injection-induced cooling is important for triggering seismicity close to the injection well and around the liquid water zone. Away from the well, on the other hand, injection-induced changes in the steam pressure appear to be the dominant cause for triggering shear reactivation and seismicity.

The predicted extent of the stimulation zone was compared with MEQ data recorded by a dedicated seismic array deployed at The Geysers. The seismic array consists of 31 three-component short-period stations with a sampling frequency of 500 Hz (Majer and Peterson 2007). In addition, 15 temporary stations have been located around the EGS demonstration area for more accurate location of events. Seismic events with magnitudes as low as 0.5 were detected located using methods derived from conventional earthquake seismology, including a few events above magnitude 2.5 (Garcia et al. 2012). Figures 13 and 14 show a comparison of the predicted extent of the stimulation zone and observed MEQ events around the P-32 injection well. The observed MEQ hypocenters in Figs. 13 and 14 include events located with horizontal and vertical error of less than 1 km (Garcia et al. 2012). In Figs. 13 and 14, one can observe good qualitative agreement between the predicted and observed extent of the stimulation zone, although observed events also occur outside and below the predicted stimulation zone. In Fig. 13, the stimulation zone of relatively high

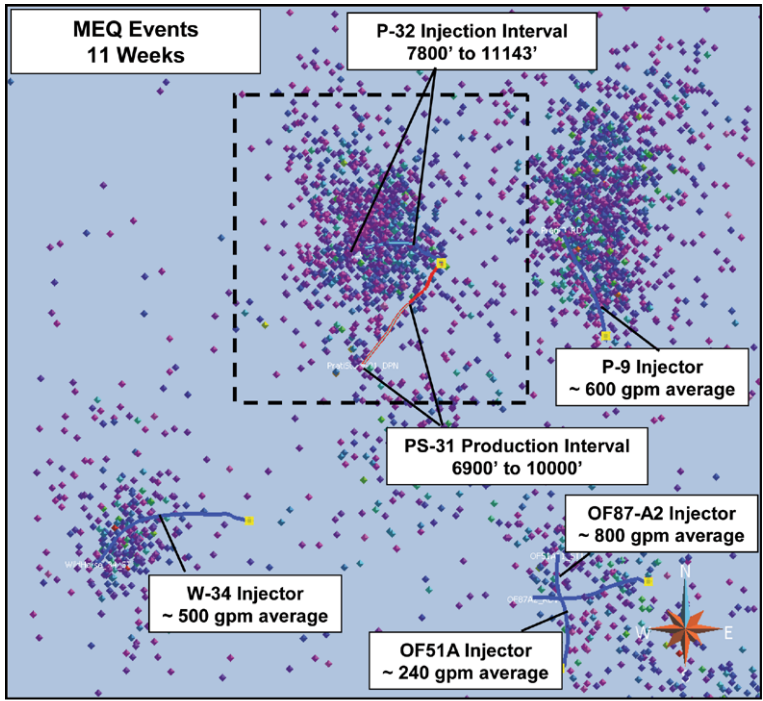
**Fig. 13** Comparison of simulated (predicted) MEQ potential (*left*) and observed locations of MEQ events (*right*) during the first 3 months of injection



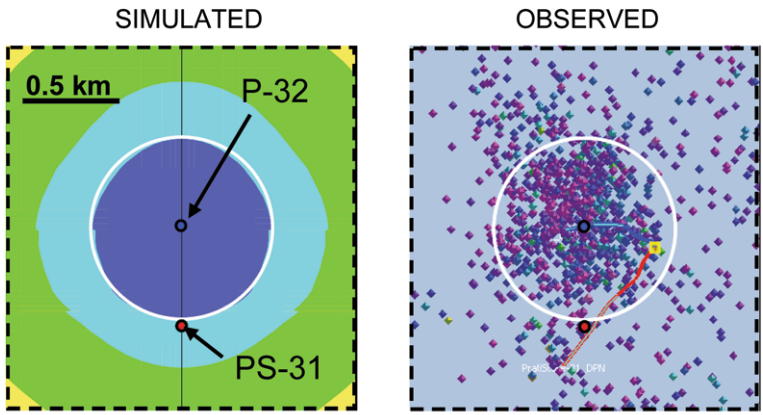
MEQ density barely reaches the PS-31 well after about 3 months, but expands more during continued injection. However, it may be concluded from Figs. 13 and 14 that the prestimulation model predicts the observed lateral extent of the stimulation zone based on MEQ distribution (at least during the first few months of injection).

## 6 Model Calibration Against Data on Reservoir Pressure and Ground Deformation

Reservoir pressure is monitored in some of the surrounding wells, including PS-31, which is located about 500 m from the P-32 injection well (Garcia et al. 2012). The observed pressure evolution at PS-31 generally correlates with the injection rate, and a distinct pressure response was specifically observed already within a few days after the start of the P-32 injection. Figure 15 presents a comparison of the simulated and observed pressure evolution for different values of reservoir porosity and permeability. It is shown that the initial pressure response occurring during the first day of injection is strongly dependent on the reservoir porosity, whereas the slope of the pressure evolution over the next 10 days is strongly dependent on the reservoir permeability. A good match between simulated and observed PS-31 pressure evolution was achieved when keeping the original permeability (Table 1), whereas the porosity had to be reduced from the original 1 % or 1.5 % (the standard value used in Calpine's reservoir models and shown in Table 1) to 0.4 %. Using the original permeability (Table 1) and 0.4 % porosity, very good agreement was achieved between simulated and observed pressure change during the first 55 days of injection, when the injection rate was kept at 400 gpm (Fig. 16). However, when the injection rate increased to 1,000 gpm, one can observe in Fig. 16 that the simulated pressure change for 0.4 % porosity slightly overshoots the observed pressure change. This may indicate that reservoir properties change during the injection. A better match for the 1,000 gpm part could be achieved by either a slight increase in permeability or an



(a)



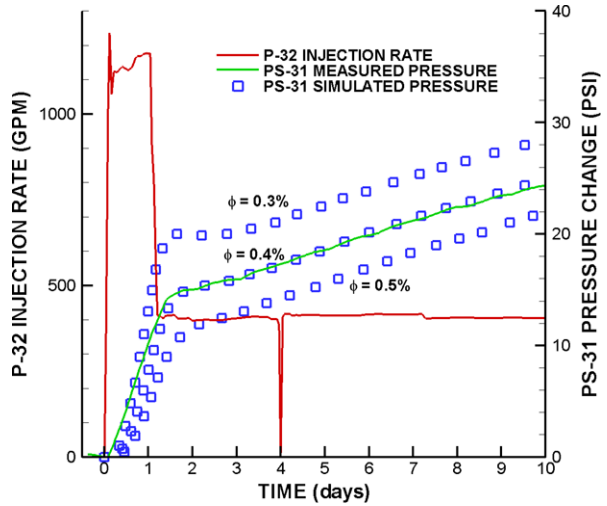
(b)

(c)

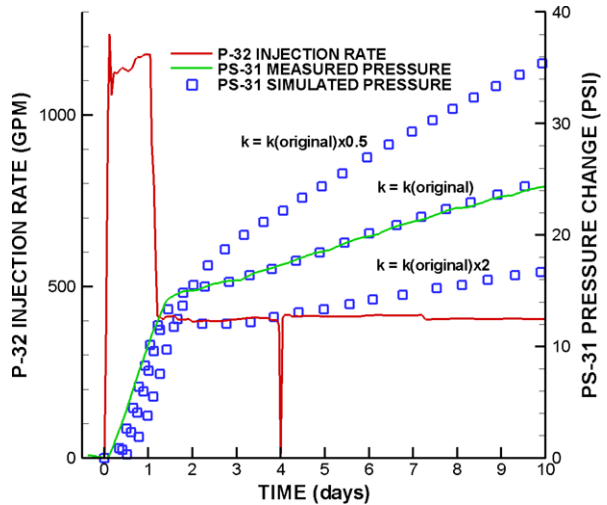
**Fig. 14** Comparison of predicted MEQ potential with observed locations of MEQ events within the first 3 months of injection, including (a) observed MEQ events around the EGS demonstration area event during 75 days of injection (Garcia et al. 2012), (b) predicted MEQ potential in which the blue contour represents the expected extent of the stimulation zone and (c) observed MEQ events around P-32 injection well

increase in porosity. The overall best match was achieved when increasing porosity from 0.4 % to 0.6 % after 55 days of injection (Fig. 16). If such an increase in porosity is what took place in the field, this would correspond to a 50 % increase in fracture

**Fig. 15** Comparison of observed and simulated pressure changes in PS-31 well located about 500 m from the P-32 injection well for the first 10 days of injection for simulations with variation in (a) porosity and (b) permeability



(a)



(b)

porosity, indicating a quite substantial effect from the stimulation, one that would increase the fracture surface area available for heat extraction. However, other features that could induce similar effects on the pressure evolution cannot be ruled out. For example, pressure around P-32 and PS-31 may be affected by heterogeneous reservoir properties and low-permeability boundaries as larger volumes of the reservoir are pressurized during the injection.

As part of the field monitoring program, LBNL commissioned TRE to perform an analysis of radar images from SAR for monitoring ground-surface deformations associated with the P-32 injection. The X-band data from Cosmo-SkyMed and TerraSAR-X satellites, with 8 to 11 days revisiting time ascending and de-

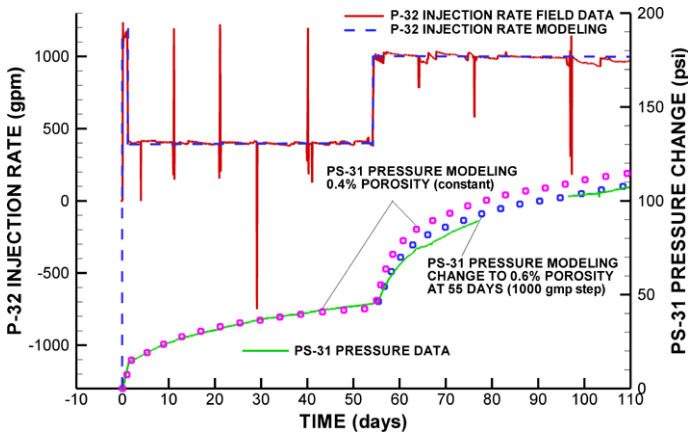


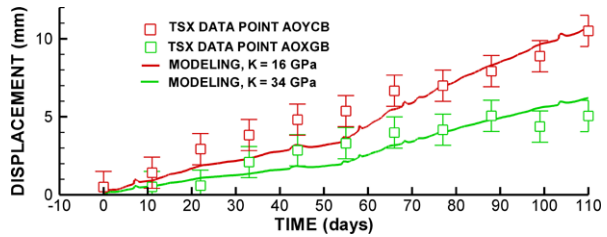
**Fig. 16** Comparison of observed and simulated pressure changes in the PS-31 well located about 500 m from the P-32 injection well over the first 110 days of injection

scending (double geometry), were acquired and analyzed by TRE using the newly developed SqueeSAR<sup>TM</sup> technique (Ferretti et al. 2011). The double geometry (ascending/descending) results in two different perspectives that increase the number of ground-measurement points, especially in a mountainous environment like The Geysers. Moreover, both vertical and horizontal (E-W) ground-displacement components can be computed. SqueeSAR<sup>TM</sup> is an evolution of the PS technique that uses both (1) permanent scatterers, such as rock outcrops and buildings and (2) spatially distributed scatterers, typically identified from homogeneous ground, scattered outcrops, debris flows, and uncultivated lands (Ferretti et al. 2011; Vasco et al. 2013).

Using X-band data from the Cosmo-Skymed and TerraSAR-X, the SqueeSAR<sup>TM</sup> analysis produced much higher density data coverage than the lower frequency C-band data over the EGS demonstration area (Vasco et al. 2013). Vasco et al. (2013) analyzed the TerraSAR-X data over the first 175 days of injection and found local ground-surface uplift that appeared to be correlated with the P-32 injection rate. When comparing this observed surface uplift to simulated results using the initial prestimulation model, it is concluded that the ground-surface uplift would be significantly overestimated when using the rock-mass bulk modulus (back-calculated from the reservoir wide analysis of the 44 years of production-induced subsidence). To match observed ground-surface uplift during the P-32 injection, the bulk modulus had to be substantially increased from the original value of  $K = 3.3$  GPa to 16 to 34 GPa.

Figure 17 shows simulated vertical displacement matched with TSX data on average range change (at a look-angle of  $29^\circ$ ) evaluated to two points, AOYCB and AOXGB, located just above the P-32 well at the distance of about 150 m from each other. To match the observed range change, the average bulk shear modulus of the rock mass had to be increased by a factor of about 5 to 10, i.e., the bulk modulus had to be increased from  $K = 3.3$  GPa to  $K = 16$  to 34 GPa. Distinctly different moduli related to subsidence and subsequent rebound uplift might be expected, considering the well-established differences between virgin and elastic reservoir compressibil-

**Fig. 17** Comparison of observed range change and simulated vertical displacement at two ground surface locations (AOYCB and AOCGB) located about 150 m apart and above the P-32 injection well (modified from Vasco et al. 2013)



ity (Teatini et al. 2011). That is, the long-term subsidence may be controlled by the tangent modulus of inelastic compaction along the virgin loading path, whereas the rebounding uplift is controlled by the elastic rock mass modulus. Moreover, the satellite data images indicate a relatively localized uplift bulge around the P-32 injection well, with a more heterogeneous uplift pattern than what could be resolved using the horizontally homogenous layered model. Indeed, the observed ground-surface uplift in AOYCB and AOCGB were significantly different, although located only 150 m from each other. This indicates that the uplift pattern could be impacted by local material heterogeneities and structures such as faults.

## 7 Comparison of Calculated MEQ Potential with Seismic Density

For a more quantitative comparison between stress modeling and observed MEQ activity, contour plots of seismic density were developed, that is the number of events per unit volume that could be directly compared to contours of calculated MEQ potential. Figures 18 and 19 present contours for such a comparison in one horizontal cross section and two vertical cross sections through the center of the stimulation zone. The contours for the field data shown in Fig. 18 were created by dividing each cross section into bins that are cube-shaped with a side length of 250 m, and recording the cumulative number of events in each bin occurring during the first 90 days of injection. Similar contours were constructed from the model simulation results using the MEQ potential expressed in terms of  $\Delta\sigma'_{1m}$  (Fig. 19). Recall that  $\Delta\sigma'_{1m} = 1.5$  MPa corresponds to the predicted extent of the stimulation zone. This is the outermost contour line in Fig. 19. Comparing the horizontal cross section in Figs. 18(a) and 19(a), one can see that this roughly corresponds to a zone with five events or more per 250 m cube volume. One can also see that closer to the center of the stimulation zone there are up to 20 events per 250 m cube, which also corresponds to areas of higher  $\Delta\sigma'_{1m}$ . For a calculated factor of 2 increase in  $\Delta\sigma'_{1m}$  (from 1.5 to 3), the observed seismic density increases by a factor of 4 (from 5 to 20 events per 250 m cube). Note, however, that in these simulations the original and softer bulk modulus of 3.3 GPa was still used, whereas a stiffer bulk modulus in the range of 16 to 34 GPa would result in much greater cooling-induced stress changes—changes that would likely increase the calculated  $\Delta\sigma'_{1m}$  in the central cooling region just around the well. In fact, the calculations indicate that cooling induced local tensile fracturing is likely in the zone of the most substantial cooling, which is around the injection well and along the liquid water zone.

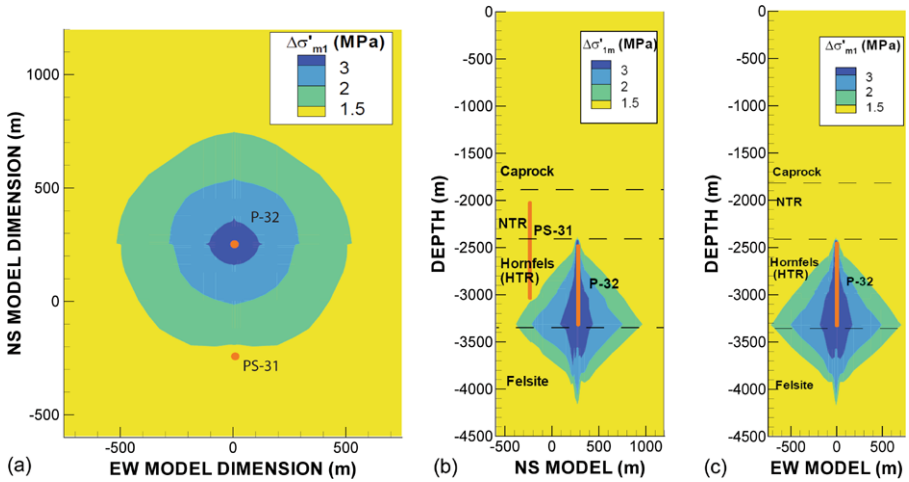


**Fig. 18** Calculated MEQ potential in terms of stress-to-strength change  $\Delta\sigma'_{1m} = \Delta\sigma'_1 - 3 \times \Delta\sigma'_3$ , presented in a (a) horizontal cross-section at 3,000 m depth, (b) north-south vertical cross-section, and (c) east-west vertical cross-section

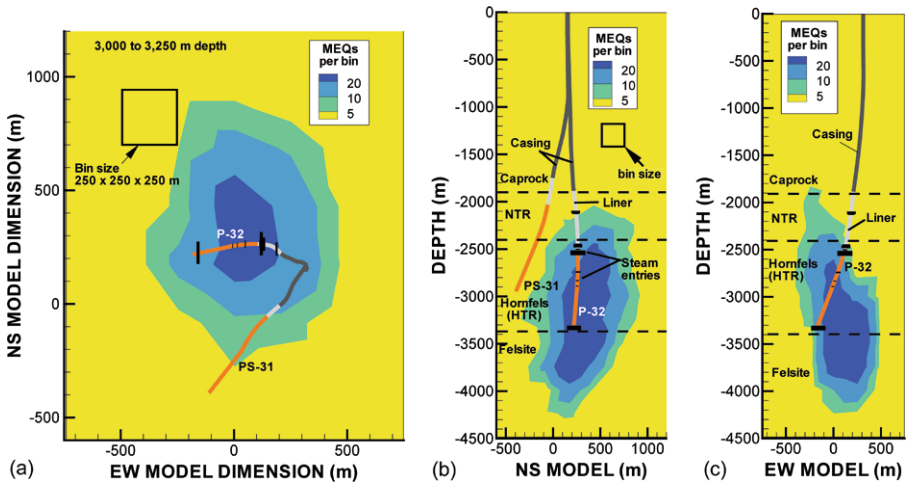


**Fig. 19** Seismic density as number of MEQ events per 250 m cube bin during the first 90 days of injection depicted in a (a) horizontal cross-section at 3,000 to 3,250 m depth, (b) north-south vertical cross-section, and (c) east-west vertical cross-section

Finally, although the agreement between the simulated and observed shape of the stimulation zone is good in the horizontal plane, one can also see that the shapes in the vertical cross sections are more heterogeneous in the field and also extend further down into the felsite (e.g., compare Figs. 18(b) with 19(b)). Indeed, in the simulation results, the blue contour does not extend further down than 3,700 m while the observed MEQ spread below 4,000 m deep into the felsite. The fact that the MEQ spreads deep into the felsite is a positive attribute and one of the goals of the project.



One way to match such deepening in the modeling would be to assign a higher vertical permeability, which could perhaps represent a vertical steam-bearing fracture zone. Moreover, field observations indicate that the MEQ zone moves slowly downwards with time along with the injection (Garcia et al. 2012). However, according to a detailed study of the daily MEQ evolution by Jeanne et al. (submitted), the shape of the stimulation zone seems to be affected by both permeable fracture zones and bounding faults in the area. This becomes more evident when studying the injection-induced MEQ evolution beyond the 90 days considered in this paper. In fact, Jeanne et al. (submitted) show that the EGS system around P-32 and PS-31 is partially confined by hydraulically bounding faults, and it will be important to include those faults when analyzing the long-term injection/production and sustainability of the EGS system.

## 8 Concluding Remarks

Coupled thermal, hydraulic, and mechanical (THM) modeling have been conducted to simulate water injection for stimulation associated with the Northwest Geysers EGS Demonstration Project, California. The numerical modeling was conducted as part of the prestimulation phase for guiding the stimulation plan. In particular, the prestimulation modeling aimed at predicting the injection-induced spatial extent of the stimulation zone as observed from monitoring of MEQ activity around the wells. Simulation results were compared to field monitoring data for the first few months of injection, including MEQ events (from a dedicated Geysers array), reservoir pressure (from the PS-31 well), and ground-surface deformation (from satellites). The results show that, with a THM model calibrated against historic injection and MEQ data at a nearby well, the model simulation could predict the observed extent of the stimulation zone, which is defined as a zone of high MEQ density around the injection well. The modeling indicates that MEQ and shear reactivation of pre-existing fractures are caused by the combined effects of injection-induced cooling and pressure changes, with the cooling being more important for triggering seismicity near the injection well and around the zone of cool liquid water. On the other hand, injection-induced changes in steam pressure are the dominant cause of seismicity farther away from the injection well. Note that these are very small changes in steam pressure, and the model simulations of pressure evolution, corroborated with pressure monitoring, indicate that reservoir pressure changes on the order of 1 MPa are sufficient to trigger a significant number of small events. This supports the notion that rock mass within The Geysers geothermal field is near critically stressed for shear failure, and that small perturbations in the stress field could induce seismicity.

Pressure-monitoring data and satellite-based ground-surface deformation data were also used to further calibrate reservoir-scale hydraulic and mechanical model properties. The pressure signature monitored from the start of the injection was particularly useful for a precise back-calculation of reservoir porosity, whereas modeling of ground-surface deformation data indicates that the reservoir has undergone strongly irreversible subsidence behavior during pressure depletion (accompanied by decreasing steam production) since the 1960s. The matching of the cross-hole pressure evolution indicates that significant increases in fracture porosity may have taken

place during the stimulation, although this cannot be conclusively stated, since other effects such as bounding faults may have affected the pressure evolution in a similar way. An irreversible subsidence behavior was indicated by the fact that a much higher modulus of the rock mass had to be assigned for matching the 1 to 1.5 cm ground uplift above the P-32 injection well. As mentioned, this indicates that the 3.3 GPa bulk modulus back-calculated from 40 years of the reservoir-wide pressure depletion and subsidence in reality represents the secant modulus of inelastic reservoir compaction, whereas during injection, the injection-induced poro-elastic reservoir expansion is controlled by the elastic rock mass bulk modulus.

Finally, although the model simulations (using a simplified geologic model) could reasonably well predict the extent of the stimulation zone, the observed MEQ evolution shows signs of more complex geology. Moreover, it was found that the stimulation zone extends deep down into the felsite, deeper than what was predicted by the numerical modeling. This indicates higher vertical permeability, through vertical permeable structures that might have been reactivated as a result of the injection. Future modeling of the site will include more detailed geology, such as steam-bearing fracture zones, bounding faults, and more exact (inclined) well traces. In fact, the field observations interpreted in Jeanne et al. (submitted) indicate that the EGS is confined by bounding semipermeable structures such as hydraulically bounding faults. It will be important to include such structures when evaluating the injection/production and long-term sustainability of the EGS. Such analysis will also include a third well, P-25 (see Fig. 2 for location) that is already producing steam and is also in contact with the stimulation zone around the P-32 well.

**Acknowledgements** This work was conducted with funding by the Assistant Secretary for Energy Efficiency and Renewable Energy, Geothermal Technologies Program, of the US Department under the US Department of Energy Contract No. DE-AC02-05CH11231, and by Calpine Corporation.

**Open Access** This article is distributed under the terms of the Creative Commons Attribution License which permits any use, distribution, and reproduction in any medium, provided the original author(s) and the source are credited.

## References

- Barton CA, Zoback MD, Moos D (1995) Fluid flow along potentially active faults in crystalline rock. *Geology* 23:683–686
- Catalli F, Meier M-A, Wiemer S (2013) The role of Coulomb stress changes for injection-induced seismicity: the Basel enhanced geothermal system. *Geophys Res Lett* 40:72–77
- Ferretti A, Prati C, Rocca F (2001) Permanent scatterers in SAR interferometry. *IEEE Trans Geosci Remote Sens* 39:8–20
- Ferretti A, Fumagalli A, Novali F, Prati C, Rocca F, Rucci A (2011) A new algorithm for processing interferometric data-stacks: SqueeSAR. *IEEE Trans Geosci Remote Sens* 49:3460–3470
- Garcia J, Walters M, Beal J, Hartline C, Pingol A, Pistone S, Wright M (2012) Overview of the northwest Geysers EGS demonstration project. In: Proceedings of the thirty-seventh workshop on geothermal reservoir engineering, Stanford University, Stanford, California, January 30–February 1, 2012
- Itasca (2009) FLAC3D, fast Lagrangian analysis of continua in 3 dimensions, version 4.0. Minneapolis, Minnesota, Itasca Consulting Group
- Jaeger JC, Cook NGW (1979) Fundamentals of rock mechanics. Chapman and Hall, London, p 593
- Khan MA, Truschel J (2010) The Geysers geothermal field, an injection success story. *GRC Trans* 34:1239–1242

- Lockner DA, Summer R, Moore D, Byerlee JD (1982) Laboratory measurements of reservoir rock from the Geysers Geothermal Field, California. *Int J Rock Mech Min Sci* 19:65–80
- Majer EL, Peterson JE (2007) The impact of injection on seismicity at the Geysers, California geothermal field. *Int J Rock Mech Min Sci* 44:1079–1090
- McClure MW, Horne RN (2012) Investigation of injection-induced seismicity using a coupled fluid flow and rate/state friction model. *Geophysics* 76:WC183
- Mossop AP, Segall P (1997) Subsidence at the Geysers geothermal field, N. California from a comparison of GPS and leveling surveys. *Geophys Res Lett* 24:1839–1842
- Nielson D, Moore JN (2000) The deeper parts of the Geysers thermal system—implications for heat recovery. *GRC Trans* 24:299–302
- Oppenheimer DC (1986) Extensional tectonics at the Geysers geothermal area, California. *J Geophys Res* 91:11463–11476
- Pruess K, Oldenburg C, Moridis G (2011) TOUGH2 user's guide, Version 2.1. LBNL-43134 (revised), Lawrence Berkeley National Laboratory, Berkeley, California
- Rutqvist J (2011) Status of the TOUGH-FLAC simulator and recent applications related to coupled fluid flow and crustal deformations. *Comput Geosci* 37:739–750
- Rutqvist J, Oldenburg C (2007) Analysis of cause and mechanism for injection-induced seismicity at the Geysers geothermal field. *GRC Trans* 31:441–445
- Rutqvist J, Oldenburg CM (2008) Analysis of injection-induced micro-earthquakes in a geothermal steam reservoir, Geysers geothermal field, California. In: Proceedings of the 42th US rock mechanics symposium, San Francisco, California, USA, June 29–July 2, 2008. American Rock Mechanics Association, San Francisco. Paper no 151
- Rutqvist J, Wu Y-S, Tsang C-F, Bodvarsson G (2002) A modeling approach for analysis of coupled multiphase fluid flow, heat transfer, and deformation in fractured porous rock. *Int J Rock Mech Min Sci* 39:429–442
- Rutqvist J, Dobson PF, Oldenburg CM, Garcia J, Walters M (2010) The northwest Geysers EGS demonstration project phase 1: pre-stimulation coupled geomechanical modeling to guide stimulation and monitoring plans. *GRC Trans* 34:1243–1250
- Schmitt AK, Grove M, Harrison TM, Lovera O, Hulen J, Walters M (2003) The Geysers–Cobb mountain magma system, California (part 2): timescales of pluton emplacement and implications for its thermal history. *Geochim Cosmochim Acta* 67:3443–3458
- Stark MA (2003) Seismic evidence for a long-lived enhanced geothermal system (EGS) in the northern Geysers reservoir. *GRC Trans* 27:727–731
- Stark MA, Box WT, Beall JJ, Goyal KP, Pingol AS (2005) The Santa Rosa-Geysers recharge project, Geysers geothermal field, California. *GRC Trans* 29:145–150
- Sternfeld JN (1989) Lithologic influences on fracture permeability and the distribution of steam in the northwest Geysers steam field, Sonoma county, California. *GRC Trans* 13:473–479
- Teatini P, Gambolati G, Ferronato M, Settari A, Walters D (2011) Land uplift due to subsurface fluid injection. *J Geodyn* 51:1–16
- Vasco DW, Rutqvist J, Ferretti A, Rucci A, Bellotti F, Dobson P, Oldenburg C, Garcia J, Walters M, Hartline C (2013) Monitoring deformation at The Geysers geothermal field, California using C-band and X-band interferometric synthetic aperture radar. *Geophys Res Lett*. doi:10.1002/grl.50314
- Walters MA, Sternfeld JN, Haizlip JR, Drenick AF, Combs J (1988) A vapor-dominated reservoir exceeding 600 °F at the Geysers Sonoma county, California. In: Proceedings of the 13th workshop on geothermal reservoir engineering, Stanford University, SGP-TR-113, pp 73–81
- Walters MA, Haizlip JR, Sternfeld JN, Drenick AF, Combs J (1991) A vapor-dominated high-temperature reservoir at the Geysers, CA. In: Monograph on the Geysers geothermal field, Geothermal Resources Council, vol 17, pp 77–87
- Williamson KH (1992) Development of a reservoir model for the geysers geothermal field. In: Monograph on the Geysers geothermal field, Geothermal Resources Council, vol 17, pp 179–187
- Williams C, Glanis SP, Moses TH, Grubb FV (1993) Heat flow studies in the northwest geysers geothermal field, CA. *GRC Trans* 17:281–288